LRP 801/05 February 2005

Probe measurements of plasma potential nonuniformity due to edge asymmetry in large-area radio-frequency reactors: the telegraph effect

A.A. Howling, L. Derendinger, L. Sansonnens,
H. Schmidt, Ch. Hollenstein, E. Sakanaka,
J.P.M. Schmitt

submitted for publication in
J. Appl. Phys.

ISSN 0458-5895

Probe measurements of plasma potential nonuniformity due to edge asymmetry in large-area radio-frequency reactors: the telegraph effect

A. A. Howling,* L. Derendinger, L. Sansonnens, H. Schmidt, and Ch. Hollenstein
Ecole Polytechnique Fédérale de Lausanne (EPFL), Centre de Recherches en Physique des Plasmas, CH-1015 Lausanne, Switzerland

E. Sakanaka and J. P. M. Schmitt
Unaxis Displays, 5 Rue Léon Blum, F-91120 Palaiseau, France
(Dated: February 21, 2005)

In large-area radio-frequency (rf) capacitive reactors, the redistribution of rf current to maintain current continuity near asymmetric sidewalls causes a perturbation in rf plasma potential to propagate along the resistive plasma between capacitive sheaths. The damping length of the perturbation can be determined by a telegraph equation. Experiments are described using a surface array of unbiased electrostatic probes in the ground electrode to verify the theoretical model of the telegraph effect in A. Howling *et al.*, J. Appl. Phys. **96**, 5429 (2004). The measured spatial dependence of the plasma potential rf amplitude and circulating non-ambipolar current agree well with two-dimensional numerical solutions of the telegraph equation. The rf plasma potential can be made uniform by using symmetric reactor sidewalls.

PACS numbers: 52.50.Dg, 52.80.Pi, 81.15.Gh

I. INTRODUCTION

Capacitively-coupled parallel plate radio-frequency (rf) reactors are commonly used for plasma-enhanced chemical vapor deposition and dry etching of thin films such as amorphous silicon or silicon oxide. Large area (> 1 m^2) reactors are used for the production of photovoltaic solar cells and thin film transistors for flat screen production. These industrial applications typically require a uniformity in film thickness to better than $\pm$ 10% - hence the interest in identifying and understanding causes of plasma nonuniformity in order to suppress them by improvements in reactor design.

The nonuniformity considered in this paper is due to the redistribution of rf current in the vicinity of reactor sidewalls to maintain rf current continuity between asymmetric electrodes. Since the lateral impedance of the plasma cannot be neglected over the long dimensions of large-area plasmas, this current redistribution results in a rf plasma potential perturbation which propagates inwards from the sidewalls along the plasma between the capacitive sheaths [1]. This is analogous to signal propagation along the lossy conductor of a transmission line, hence we call this the 'telegraph effect' following Schmitt *et al.* [2]. The damping length of the perturbation can be determined with the telegraph equation. The spatial variation in plasma potential rf amplitude results in local non-ambipolar current flow across the sheaths. In this work, the spatial dependence of the plasma potential rf amplitude and the non-ambipolar current are both measured using a surface array of electrostatic probes in the ground electrode. The experimental results are compared with a numerical solution of the telegraph equation for the rf plasma potential perturbation. An argon plasma is studied to avoid deposition on the probes and to eliminate extraneous sources of nonuniformity due to reactive gas plasmas, such as gas depletion in an inappropriate gas flow distribution [3], or the formation of nonuniform dust clouds suspended in the plasma [4, 5].

Various electromagnetic modes can cause plasma nonuniformity. These include the standing wave mode (associated with high frequencies in large reactors [2, 6–14]), edge-localized modes at the junction between the ground and excitation electrodes [1, 9], and the telegraph effect [1, 2]. All of these modes arise simultaneously in the wavefield solution for plasma in an asymmetric reactor [13]. To avoid standing wave nonuniformity in the parallel-plate reactor, the rf frequencies used in this work are low enough, and the reactor small enough, such that the rf wavelength is much longer than the reactor dimensions, even when the wavelength reduction factor [9, 13] due to the presence of the plasma is accounted for. Conducting electrode surfaces are therefore equipotential for the rf, as well as the dc, voltages over their whole surface. To summarize, the experiments are designed to study the influence of edge asymmetry on plasma potential nonuniformity in the absence of other perturbations except for edge-localized modes.

This paper is organized as follows: Sec. II describes the rf plasma reactor, the surface array of electrostatic probes, and the probe diagnostic method used to measure the spatial variation in plasma potential rf amplitude. In Sec. III, a two-dimensional numerical solution gives the spatial dependence of the plasma potential rf amplitude determined by the telegraph equation. The experimental results are compared with the numerical solution in Sec. IV before concluding.

*Electronic address: alan.howling@epfl.ch

II. EXPERIMENTAL ARRANGEMENT

The plasma reactor shown schematically in Fig. 1 is a modified version of an industrial KAI-S type PlasmaBox® reactor. The 462 mm × 562 mm excitation electrode, which also serves as the uniform gas showerhead, is suspended inside the grounded reactor box above the grounded reactor floor (470 mm × 570 mm) with a 25 mm-high inter-electrode gap. The whole system is contained within a steel vacuum chamber. Pure argon at 0.1 - 0.5 mbar pressure was used at flowrates of 100 - 400 sccm and the reactor was at ambient temperature. The reactor and probes were made of aluminum; insulator parts were made of alumina.

For the rf excitation frequencies used, 27.12 MHz or 40.68 MHz, the free space wavelengths are 11.05 m and 7.37 m respectively. Even with the wavelength reduction factor of $\lesssim 3$ [9, 13], the effective rf wavelength is sufficiently larger than the electrode lateral dimensions so that standing wave effects can be neglected as a cause of plasma nonuniformity in this work where the rf power is capacitively coupled to the rf electrode backface center [8]. The absence of standing wave nonuniformity is also shown by the profile measurements in Sec. IV. The rf excitation voltage was measured directly at the excitation electrode using a wideband (dc - 100 MHz) voltage probe.

A. Electrostatic probes and signal acquisition

The ground electrode surface contains 68 planar electrostatic probes in two groups:

a) 47 circular probes (10 mm diameter) in a more-or-less regular two-dimensional array, within mechanical constraints, to give an average spatial resolution of about 70 mm over the whole surface of the ground electrode.

b) 21 smaller probes (4 mm diameter) in 3 rows of 7 near two corners and an edge with a 10 mm spacing for better spatial resolution near to the sidewalls.

The probe arrangement is shown on the base-plane of the measurement figures, for example, Fig. 8, in Sec. IV. Each probe head is isolated from the ground electrode by an alumina sleeve.

The aim is to compare measurements of the spatial dependence of the plasma potential rf amplitude with a numerical solution of the telegraph equation. Measurements of the rf plasma potential in rf plasma reactors generally require special rf probe techniques or precautions to eliminate stray rf currents and induced rf voltages [15–17]. Furthermore, an array of probes across the whole plasma area would be impractical and perturbing in a large-area parallel-plate reactor. In this work, dc currents and dc voltages are monitored - thereby avoiding problems of rf measurements - at the ground electrode using a convenient, non-invasive, surface probe array. Circulating dc currents and dc probe voltages are predicted as a consequence of the telegraph effect [1] and these dc values are used here to compare experiment and theory.

In Fig. 1, each probe connection wire has a coaxial screen connected to ground next to the probe itself. Effective rf grounding of each probe was assured by the combined capacitance of the probe head ($\sim$ 13 pF) and its coaxial cable ($\sim$ 50 pF). The total capacitance to ground of each probe is therefore much larger than its sheath capacitance to the plasma which is less than 1 pF. This rf grounding ensured continuity of the rf current from plasma to ground via the probes so that the probe surfaces form an integral part of the ground electrode at the excitation frequency, with negligible probe rf voltage. The probe rf current is thus de-coupled from the dc measurement circuit of each probe. The probe capacitance was judged to be sufficient for this because a supplementary 1 nF capacitor across the probe connections made no difference to the dc measurements. A schematic of the probe array and signal acquisition is shown in Fig. 1. The coaxial cables are led via vacuum feedthroughs to pairs of electromechanical relays arranged in multiplexers (National Instruments (NI) PXI-2503, appropriate for low-level signals) and a high performance $6\frac{1}{2}$ digit multimeter (NI PXI-4070 for dc voltage and dc current measurements) in a PXI crate with a LabVIEW software interface. The selected precision for these experiments was 10 nA for the dc current measurements, and 10 μV for the dc voltage measurements. Using hardware-handshaking between the multimeter and multiplexers, the time for one measurement cycle of all the probes was about 30 seconds, allowing for relay switching time, ADC self-calibration, auto-zero time, relay settling, and a 100 ms signal acquisition time window for each measurement of each probe. The signals were highly reproducible indicating negligible spurious electrical interference, so that cycle averaging was unnecessary and all the measurements presented are raw data from one-shot acquisitions with no data smoothing. The per cent relative standard deviation over ten consecutive acquisition cycles was less than 2.5% for voltage measurements and 5% for current measurements with the large probes (3.5 and 7% respectively for the small probes), and this variation was principally due to drift in the plasma parameters. The (dc) saturated ion current measurements were obtained by inserting a battery at the multimeter current terminal to give a -30 V bias on each probe during its measurement cycle. The polarity of the current flow in this work is such that net positive ion current from the plasma to the probe is positive.

The probe surfaces must be conducting since insulating layers would invalidate dc potential and dc current measurements. The electrodes and probes were mechanically polished and only exposed to plasmas of argon and hydrogen. No deposition or probe discoloration was observed after four months of plasma experiments.

B. Probe diagnostic method

The primary aim is to measure the two-dimensional profile of the variation in the plasma potential rf amplitude, $\Delta\tilde{u}_p(x,y)$, due to electrode edge asymmetry, which will then be used to compare with the two-dimensional numerical solution of the telegraph equation obtained in Sec. III. Here we will show that the surface probe *dc* floating potentials can be used to estimate the spatial variation in the *rf amplitude* of the plasma potential [18]. In the previous section it was shown that the probes are effectively rf-grounded and consequently have no rf voltage component. On the other hand, the input impedance of the digital multimeter for the measurement of dc voltage is greater than 10 GΩ. The measured probe voltage is therefore the dc floating potential.

Firstly, we briefly revise a conventional model for the self-rectification voltage across a sheath in presence of rf excitation [19–22]. For a symmetric reactor with uniform (unique) plasma potential, and a sinusoidal rf excitation of amplitude $\tilde{u}_{rf}$, the plasma potential can be written as

$$U_{sym}(t) = \bar{U}_{sym} + \frac{\tilde{u}_{rf}}{2}\cos\omega t, \quad (1)$$

making the approximation of purely capacitive sheaths and negligible transverse plasma impedance for which $\tilde{u}_{rf}/2$ is the amplitude of the rf plasma potential, and $\bar{U}_{sym}$ is the dc plasma potential. For a rf external circuit with a dc-blocking capacitor, the condition for zero net conduction current to the ground electrode is that the ion saturation current equals the time-averaged electron current. Using conventional expressions [22] and assuming a Maxwellian distribution for the electrons, we obtain

$$I_e^{\mathrm{sat}}\langle\exp(-U_{sym}(t)/T_e)\rangle = I_i^{\mathrm{sat}}, \quad (2)$$

where I_i^{sat} and I_e^{sat} are respectively the ion and electron saturation currents, T_e is the electron temperature in volts, and the angular brackets signify the time-average over an rf cycle. Substituting for the plasma potential $U_{sym}(t)$ gives

$$\exp\left(\frac{-\bar{U}_{sym}}{T_e}\right)\langle\exp\left(\frac{-\tilde{u}_{rf}\cos\omega t}{2T_e}\right)\rangle\sqrt{\frac{M_i}{2.3m_e}} = 1, \quad (3)$$

where the square root term is a commonly-used ratio of the electron and ion saturated currents. Performing the time-averaging by means of the relation $\mathbf{I}_0(a) = (1/\pi)\int_0^{\pi}\exp(\pm a\cos\theta)\,d\theta$, where $\mathbf{I}_0$ is the zeroth order modified Bessel function of the first kind and a the magnitude of the sinusoidal term [23], gives

$$\exp\left(\frac{-\bar{U}_{sym}}{T_e}\right)\mathbf{I}_0\left(\frac{\tilde{u}_{rf}}{2T_e}\right)\sqrt{\frac{M_i}{2.3m_e}} = 1, \quad (4)$$

or, by taking the logarithm,

$$\bar{U}_{sym} - T_e\ln\left[\mathbf{I}_0\left(\frac{\tilde{u}_{rf}}{2T_e}\right)\right] - \frac{T_e}{2}\ln\left(\frac{M_i}{2.3m_e}\right) = 0. \quad (5)$$

This is the self-rectification condition which the dc plasma potential $\bar{U}_{sym}$ must satisfy for zero time-averaged current density (ambipolarity) everywhere over the ground electrode in a symmetric reactor. The plasma potential referenced to ground is the same as the ground electrode sheath voltage in this model. Since the probe floating potential measurement also imposes zero dc current to each probe, the sheath voltage of the probes is the same as the ground electrode sheath voltage, hence the measured probe floating potential with respect to ground would be zero for all the probes in a symmetric reactor.

The asymptotic expansion $\mathbf{I}_0(a) = \exp(a)/\sqrt{2\pi a}$ gives a very good approximation [23] when $\tilde{u}_{rf}/2 \gtrsim 5T_e$ (see Appendix), whereupon Eq. (5) can be rewritten as

$$\bar{U}_{sym} - \frac{\tilde{u}_{rf}}{2} + \frac{T_e}{2}\ln 2\pi\left(\frac{\tilde{u}_{rf}}{2T_e}\right) - \frac{T_e}{2}\ln\left(\frac{M_i}{2.3m_e}\right) \simeq 0. \quad (6)$$

To describe a perturbation to the rf plasma potential, we now introduce a general spatial perturbation, at the excitation frequency, of complex amplitude $\tilde{\mathbf{v}}(\underline{x})$ where $\underline{x} = \{x, y\}$. We will assume that $|\tilde{\mathbf{v}}(\underline{x})| \ll \tilde{u}_{rf}$, so that this perturbation leaves the plasma potential uniform to first order (concerning the telegraph effect, this is satisfied for nearly-symmetric reactors whose lateral dimensions are much larger than the inter-electrode gap [1]; this is why we consider large-area reactors). The modified plasma potential, $U_p(\underline{x}, t)$, in comparison with Eq. (1), is

$$U_p(\underline{x}, t) = \bar{U}_p + \frac{\tilde{u}_{rf}}{2}\cos\omega t + \Re\left[\tilde{\mathbf{v}}(\underline{x})\exp(i\omega t)\right], \quad (7)$$

or equivalently,

$$U_p(\underline{x}, t) = \bar{U}_p + \tilde{u}_p(\underline{x})\cos(\omega t + \psi(\underline{x})), \quad (8)$$

where

$$\tilde{u}_p(\underline{x}) = \left|\tilde{u}_{rf}/2 + \tilde{\mathbf{v}}(\underline{x})\right| \quad (9)$$

is the rf amplitude (magnitude) of the perturbed plasma potential. The modified dc plasma potential $\bar{U}_p$ is taken to be uniform because the dc conduction current is much less than the rf conduction current in the plasma bulk [1]; the uniformity of the plasma dc potential in the presence of a nonuniform plasma rf potential has also been recently demonstrated experimentally by Perret *et al.* [24]. Since the conducting ground electrode is equipotential, the sheath dc voltage is therefore also uniform. In the presence of any spatial variation of plasma potential rf amplitude (for example, due to the telegraph or standing wave effects [18]) it is now impossible to simultaneously satisfy the self-rectification condition, Eq. (5), everywhere on the ground electrode surface. In this case, there is local non-ambipolarity and dc current will circulate within the reactor between the plasma and conducting electrode surfaces [1, 18, 24, 25]. The net dc current in the external circuit is still zero, imposed by the dc-blocking capacitor, because the surface integral of the

circulating dc current to each electrode remains zero by self-adjustment of the dc plasma potential, from $\bar{U}_{sym}$ to $\bar{U}_p$, to maintain global ambipolarity (see Ref. [1]). Local non-ambipolarity was also measured using surface electrostatic probes by Mümken and Kortshagen [26] in an inductively coupled plasma, where the non-ambipolarity was due to nonuniformities in ion density and electron distribution function. In contrast, the plasma density and electron temperature in this work are considered uniform to first order, and the local non-ambipolarity is due to nonuniformity of the plasma potential rf amplitude.

The dc floating potential of the probes for the perturbed plasma potential is no longer zero because the self-rectification condition in Eq. (5) is locally not satisfied for grounded surfaces. Instead, each probe reaches a dc floating potential, $\bar{V}_f(\underline{x}) \neq 0$, different from the ground electrode, in order to satisfy local ambipolarity appropriate to the *local* plasma potential. Re-writing Eq. (2) for zero dc current to a probe in the presence of the modified plasma potential, we obtain an expression for the dc floating potential $\bar{V}_f(\underline{x})$ as follows:

$$I_e^{\mathrm{sat}}\langle \exp(-[U_p(\underline{x},t) - \bar{V}_f(\underline{x})]/T_e)\rangle = I_i^{\mathrm{sat}}, \qquad (10)$$

where $[U_p(\underline{x},t) - \bar{V}_f(\underline{x})]$ is the modified sheath potential at a floating potential probe which replaces the sheath potential $U_{sym}(t)$ in Eq. 2. Repeating the time-averaging procedure (where all phase information is lost), the local self-rectification version of Eq. (5) becomes

$$\bar{U}_p - T_e \ln\left[\mathrm{I}_0\left(\frac{\tilde{u}_p(\underline{x})}{T_e}\right)\right] - \frac{T_e}{2}\ln\left(\frac{M_i}{2.3m_e}\right) = \bar{V}_f(\underline{x}). \qquad (11)$$

The asymptotic expansion version of Eq. (6) is now

$$\bar{U}_p - \tilde{u}_p(\underline{x}) + \frac{T_e}{2}\ln 2\pi\left(\frac{\tilde{u}_p(\underline{x})}{T_e}\right) - \frac{T_e}{2}\ln\left(\frac{M_i}{2.3m_e}\right) \simeq \bar{V}_f(\underline{x}). \qquad (12)$$

Subtracting Eq. (12) from Eq. (6) gives

$$-\bar{V}_f(\underline{x}) \simeq \tilde{u}_p(\underline{x}) - \frac{\tilde{u}_{rf}}{2} + \bar{U}_{sym} - \bar{U}_p - \frac{T_e}{2}\ln\left[\frac{\tilde{u}_p(\underline{x})}{\tilde{u}_{rf}/2}\right]. \qquad (13)$$

By series expansion, the magnitude of the logarithmic term is $\leq (T_e/\tilde{u}_{rf})|\tilde{\mathrm{v}}(\underline{x})|$; this is an order of magnitude smaller than $|\tilde{\mathrm{v}}(\underline{x})|$ for $\tilde{u}_{rf} \gtrsim 10T_e$, which is the same condition as for the asymptotic expansion in Eq. (6). Therefore the logarithmic term can be neglected to first order in $|\tilde{\mathrm{v}}(\underline{x})|$ and we finally obtain:

$$-\bar{V}_f(\underline{x}) \simeq \triangle\tilde{u}_p(\underline{x}) - \triangle\bar{U}_p, \qquad (14)$$

where

$$\triangle\tilde{u}_p(\underline{x}) = \tilde{u}_p(\underline{x}) - \tilde{u}_{rf}/2 = \left|\tilde{u}_{rf}/2 + \tilde{\mathrm{v}}(\underline{x})\right| - \tilde{u}_{rf}/2 \qquad (15)$$

is the perturbation to the plasma potential rf amplitude of the asymmetric reactor with respect to the case of symmetric electrodes, and

$$\triangle\bar{U}_p = \bar{U}_p - \bar{U}_{sym} \qquad (16)$$

is the uniform, dc level shift of the plasma dc potential with respect to the case of symmetric electrodes. Note that only $-\bar{V}_f(\underline{x})$ and $\triangle\tilde{u}_p(\underline{x})$ are spatially dependent. In this way, a $\{x, y\}$ measurement of the negative of the measured dc floating potential, $-\bar{V}_f(\underline{x})$, can be used to compare with the spatial dependence of the perturbation to plasma potential rf amplitude. This relation will be used in Sec. IV to compare the $-\bar{V}_f(\underline{x})$ measurements with the numerical solution of the telegraph equation for $\triangle\tilde{u}_p(\underline{x})$ obtained in Sec. III. The accuracy of the approximations made above, including the assumption of sinusoidal sheath voltage, is considered in the Appendix.

The physical principle of the floating probe measurement can be summarized as follows: the ambipolar sheath at a floating probe fixes the self-rectification relation between the sheath dc and rf voltage components. The plasma dc potential is uniform, and the floating probe rf potentials are all zero. Therefore, the spatial variation of the plasma potential *rf amplitude* can only be matched by the spatial variation of the floating probe *dc* potential. Consequently, the nonuniformity of the plasma rf potential can be deduced from the nonuniformity of the floating probe dc potential, which is conveniently measured. This method has also been used to measure the rf plasma potential nonuniformity due to the standing wave effect [18].

Another aim is to use the probe array to measure the local non-ambipolar dc current, circulating via the plasma and conducting electrode surfaces, which is inherent in the telegraph effect [1]. The digital multimeter can also be used to measure the probe dc current. As mentioned above, the rf current flows directly to ground via the probe-to-ground capacitance, but now dc current can flow to ground via the low dc-input-impedance of the multimeter, which maintains the probe dc voltage at zero. This grounded probe dc current, $\bar{I}_{gnd}$, can be calculated from the difference in ion saturation current and time-averaged electron current to the probe by setting $\bar{V}_f = 0$ in Eq. (10):

$$\bar{I}_{gnd}(\underline{x}) = I_i^{\mathrm{sat}} - I_e^{\mathrm{sat}}\langle \exp(-U_p(\underline{x},t)/T_e)\rangle. \qquad (17)$$

Repeating the rf cycle-averaging procedure gives the local non-ambipolar current

$$\bar{I}_{gnd}(\underline{x}) = I_i^{\mathrm{sat}}\left[1 - \sqrt{\frac{M_i}{2.3m_e}}\exp\left(\frac{-\bar{U}_p}{T_e}\right)\mathrm{I}_0\left(\frac{\tilde{u}_p(\underline{x})}{T_e}\right)\right], \qquad (18)$$

which can be used to compare the grounded probe dc current measurement $\bar{I}_{gnd}(\underline{x})$ with the plasma potential rf amplitude $\tilde{u}_p(\underline{x})$ from the numerical solution of the telegraph equation.

Any nonuniform plasma potential rf amplitude (in the presence of a uniform dc plasma potential [24]), whether due to telegraph [18], standing wave [18, 24, 25] or other effects, separately or simultaneously, will give rise to circulating dc currents and non-zero floating probe dc potentials.

III. NUMERICAL MODEL OF THE TELEGRAPH EFFECT

The previous paper on the telegraph effect [1] used a one-dimensional Cartesian analytical model to give a physical description of the phenomena involved. For this, it was necessary to consider a reactor infinitely long and uniform in the other dimension. For the rectangular reactor used for experiments in this paper, however, the proximity of the lateral walls and corners have a strong influence, depending on the value of the damping length, and so a two-dimensional numerical solution is now necessary. The model in Ref. [1] makes several simplifying assumptions, such as constant sheath width, uniform plasma density and electron temperature and therefore does not give a self-consistent treatment of the plasma, but assumes that the telegraph nonuniformity of the plasma potential is only a first-order perturbation which leaves the plasma approximately uniform. The plasma is treated as a sheet, with no vertical structure, having a lateral resistance per square, $R_{sq} = m_e\nu_m/(n_e e^2 h)$ (where ν_m is the electron-neutral collision frequency and h the plasma sheet height), and lateral inductance per square, $L_{sq} = R_{sq}/\nu_m$, as shown in the equivalent circuit schematic of Fig. 2. To maintain rf displacement current continuity between the electrode sheaths, the sidewall sheath rf displacement current generates a lateral rf sheet conduction current $\underline{I}(\underline{x},t)$ per unit electrode width in the plasma, integrated over the plasma bulk height h, which is redistributed to the electrodes via the capacitive sheaths. This causes a perturbation $V(\underline{x},t) = \tilde{\mathrm{v}}(\underline{x})e^{i\omega t}$, where $\tilde{\mathrm{v}}(\underline{x})$ is a complex amplitude, so that the amplitude of the perturbed rf plasma potential is

$$\tilde{u}_p(\underline{x}) = \left|\tilde{u}_{rf}/2 + \tilde{\mathrm{v}}(\underline{x})\right|, \quad (19)$$

as defined previously in Eq. (9). Note that the ground sheath voltage is identical to the plasma potential because the latter is referenced to ground. The magnitude of the rf voltage across the excitation electrode sheath is $\left|\tilde{u}_{rf}/2 - \tilde{\mathrm{v}}(\underline{x})\right|$. From Fig. 2 and Ref. [1], the equations for $V(\underline{x},t)$ are

$$\nabla V = -L_{sq}\frac{\partial \underline{I}}{\partial t} - R_{sq}\underline{I} \quad \text{and} \quad \nabla . \underline{I} = -C'\frac{\partial V}{\partial t}, \quad (20)$$

where $C' = 2\epsilon_0/d$ is the parallel combination of ground and excitation sheath capacitances per unit area [1]. The voltage perturbation is therefore given by

$$\nabla^2 V - L_{sq}C'\frac{\partial^2 V}{\partial t^2} - R_{sq}C'\frac{\partial V}{\partial t} = 0, \quad (21)$$

which is the two-dimensional telegraph equation. The lateral rf current flow along the plasma between the sheaths which isolate the plasma from the electrodes is analogous to rf current flow along a coaxial cable which has a lossy central conductor; the sheaths represent the dielectric medium of the coaxial cable. The name "telegraph equation" specifically applies to signal transmission along a lossy transmission line.

The equation to be solved numerically is

$$\nabla^2 \tilde{\mathrm{v}} = \frac{2}{\delta^2}\left(i - \frac{\omega}{\nu_m}\right)\tilde{\mathrm{v}}, \quad (22)$$

where δ is a damping scale-length for the telegraph perturbation which can be written as [1]:

$$\delta = \sqrt{\frac{2}{\omega R_{sq} C'}} = \omega_{pe}\sqrt{\frac{hd}{\omega \nu_m}}, \quad (23)$$

where ω_{pe} is the electron plasma frequency and d the sheath width; the inter-electrode gap is $h + 2d$. A purely resistive plasma approximation ($\omega/\nu_m \ll 1$) was made in Ref. [1] to facilitate an analytical solution. The capacitive coupling of the plasma via a sidewall sheath at a grounded sidewall causes a lateral rf conduction current perturbation in the plasma

$$I\big|_{wall} = C_{wall}\frac{\partial U_p}{\partial t}\bigg|_{wall} = i\omega C_{wall}\left(\frac{\tilde{u}_{rf}}{2} + \tilde{\mathrm{v}}\big|_{wall}\right)e^{i\omega t}, \quad (24)$$

where $C_{wall} = \epsilon_0 H/d_{wall}$ is the wall sheath capacitance per unit electrode width [1]. Substitution into the equation for ∇V in Eq. (20) defines the boundary condition

$$\hat{n}\cdot\nabla\tilde{\mathrm{v}}\big|_{wall} = -i\omega R_{sq}C_{wall}\left(1 + i\frac{\omega}{\nu_m}\right)\left(\frac{\tilde{u}_{rf}}{2} + \tilde{\mathrm{v}}\big|_{wall}\right), \quad (25)$$

where $\hat{n}$ is a normal unit vector directed outwards from the walls. By substituting the solution for $\tilde{\mathrm{v}}(\underline{x})$ into Eq. (19) to obtain $\tilde{u}_p(\underline{x})$, the telegraph perturbation to the plasma potential rf amplitude of the asymmetric reactor with respect to a symmetric reactor can be calculated, $\Delta\tilde{u}_p(\underline{x}) = \tilde{u}_p(\underline{x}) - \tilde{u}_{rf}/2$, which is the same as Eq. (15).

The dc plasma potential $\bar{U}_{sym}$ for a symmetric reactor is given by Eq. (5). The dc plasma potential $\bar{U}_p$ for the asymmetric reactor is calculated by integrating the local non-ambipolar current, Eq. (18), over the whole grounded surface, and adjusting the dc plasma potential for zero net current as imposed by the dc-blocking capacitor in the external rf circuit [1]. Hence we obtain $\Delta\bar{U}_p = \bar{U}_p - \bar{U}_{sym}$, which is the same as Eq. (16). The telegraph model can then be tested against experiment by comparing the measurement of $-\bar{V}_f(\underline{x})$ with the telegraph calculation of $\Delta\tilde{u}_p(\underline{x}) - \Delta\bar{U}_p$ via Eq. (14). The self-bias voltage can also be calculated by adjustment for zero net current to the excitation electrode [1] and compared with the measured value.

IV. PROBE MEASUREMENTS AND COMPARISON WITH THE TELEGRAPH MODEL

The measured spatial profile of the perturbation to the plasma potential rf amplitude is estimated by interpolation of the negative of the probe dc floating potential measurements, $-\bar{V}_f(\underline{x})$. The interpolation method [27]

produces a smooth surface which always goes through the data points, and extrapolates to the reactor edges. The figures for the measurements therefore have no fitting parameters and simply represent a surface interpolated from the raw data on a 35×35 line grid.

The calculated spatial profile of the perturbation to the plasma potential rf amplitude is given by the numerical solution of the telegraph equation Eq. (22). The form of the spatial variation depends only on the damping scale-length δ which is determined by the experimental parameters via Eq. (23). The excitation angular frequency is $\omega = 2\pi f$; the electron-neutral collision frequency is proportional to the argon pressure p (using ν_m [s^{-1}]$\approx 6 \cdot 10^9 p$ [mbar]); and the electron plasma frequency $\omega_{pe} = (n_e e^2/\epsilon_0 m_e)^{1/2}$, where n_e [m^{-3}] is the electron density. The latter can be inferred approximately from the probe measurements of saturated ion current density via $J_{\rm sat}[{\rm Am}^{-2}] \approx 0.61 e n_e (eT_e/M_i)^{1/2}$ (the electron temperature T_e is taken to be 2 V; M_i[kg] is the argon ion mass). In terms of the experimental parameters, the expression for the damping length in Eq. (23) can be rewritten in convenient units as:

$$\delta[{\rm mm}] \approx 20\sqrt{\frac{J_{\rm sat}[{\rm Am}^{-2}]d[{\rm mm}](25-2d)}{f[{\rm MHz}]p[{\rm mbar}]}}. \qquad (26)$$

The damping length is therefore determined by known or estimated experimental parameters except for the sheath width d (substituting for h using $h + 2d = 25$ mm, the inter-electrode gap). The sheath width d is therefore a free parameter for δ; its value was chosen to give the damping length which gave the form of the numerical solution closest to the measured voltage profiles.

The magnitude of the perturbation is determined by the current from the sidewall sheath in Eq. (24); it is proportional to the measured rf amplitude of the excitation electrode voltage, $\tilde{u}_{rf}$, and the wall sheath capacitance per unit electrode width, $C_{wall} = \epsilon_0 H/d_{wall}$. This latter fitting parameter therefore depends on the effective width of the sidewall sheath, $d_{wall} \simeq d$. This sheath might be wider than the lateral electrode sheath due to poor contact of the plasma with the sidewall (for example, for low power plasmas), or narrower due to more intense edge plasma (for example, due to fringing field effects at the electrode edges in high power plasmas). In practice, the best fits to the measured amplitudes were given by $d_{wall} \simeq 1.5d$ for the low power experiments (short δ), and $d_{wall} \simeq 0.8d$ for the high power experiments (long δ).

In each of Secs. IV A to IV D below, two plasma conditions were chosen to investigate the plasma potential rf amplitude profile, corresponding to a short and a long telegraph damping scale-length:

i) Short damping length, $\delta \approx 33$ mm. Plasma parameters: excitation frequency 40.68 MHz, argon pressure 0.5 mbar, measured ion saturation current density ≈ 0.8 Am^{-2} for which the estimated plasma density was $n_e \approx 3.7 \cdot 10^{15}$ m^{-3}. These plasma conditions were obtained for 60 W rf input power and rf voltage amplitude of $\tilde{u}_{rf} \sim 24$ V measured at the excitation electrode. The sheath widths chosen were $d = 4$ mm and $d_{wall} = 1.5d$, which is physically reasonable for this very low voltage plasma.

ii) Long damping length, $\delta \approx 105$ mm. Plasma parameters: excitation frequency 27.12 MHz, argon pressure 0.1 mbar, measured ion saturation current density ≈ 1.8 Am^{-2} for which the estimated plasma density was $n_e \approx 8.4 \cdot 10^{15}$ m^{-3}. These plasma conditions were obtained for 200 W rf input power and rf voltage amplitude of $\tilde{u}_{rf} \sim 140$ V measured at the excitation electrode. The sheath widths chosen were $d = 2$ mm and $d_{wall} = 0.8d$ for this higher power plasma.

These two groups of experimental parameters, along with the fixed estimates for d and d_{wall}, were used for all the numerical simulations in Secs. IV A to IV D, with no other fitting parameters.

A. Asymmetric reactor: ground electrode area larger than the excitation electrode area

The reactor asymmetry shown schematically in Fig. 3 is due to the 25 mm-high grounded sidewalls on all four sides. The total grounded area is therefore larger than the excitation electrode area, which is a conventional asymmetry situation in rf plasma processing where the excitation electrode is commonly placed inside a grounded enclosure. Ref. [1] considers the same reactor geometry.

Fig. 3(a) shows the negative of the probe dc floating potential measurements which approximately represent the spatial variation of the plasma potential rf amplitude according to Eq. (14). Fig. 3(b) shows the numerical solution of the spatial dependence of the plasma potential rf amplitude using the telegraph equation and the parameters described above. The good agreement between these measured and calculated profiles is an experimental verification of the telegraph effect in this large area reactor. These profiles were obtained for the case of short damping length, δ =33 mm. The plasma potential rf amplitude decreases near to the boundaries over a distance $\approx$100 mm $\approx 3\delta$ in order to reduce the rf current density across the ground electrode sheath - this is necessary to maintain rf current continuity between the electrodes when the ground electrode has a larger area [1]. The relative drop in plasma potential rf amplitude is especially marked in the corners, $\triangle\tilde{u}_p/(\tilde{u}_{rf}/2) \approx 20\%$, because of the influence of the adjacent sidewalls which sharply increases the local area asymmetry over the length-scale of the telegraph damping length - this is a two-dimensional effect [18] which is reproduced by the two-dimensional numerical simulation. As a result, the sheath rf voltage amplitude at the reactor corners is reduced by $\approx 20\%$ at the ground electrode, and increased by a similar amount at the excitation electrode, with respect to the unperturbed value, $\tilde{u}_{rf}/2$, at the reactor center [1]. Assuming local power dissipation proportional to the sum of the

square of the sheath rf voltages, the total power density at the reactor corners therefore increases by about 4% with respect to the reactor center. The local power densities of the individual sheaths at the ground and excitation electrode corners, however, are respectively $\sim 64\%$ and $\sim 144\%$ of the central, symmetric sheath power density. The telegraph effect can therefore cause a significant edge plasma perturbation for an asymmetric sidewall height which is only $\sim 5\%$ of the electrode width.

We are principally interested in the form and amplitude of the spatial dependence in Eq. (14), although the dc levels in the figures and the measured and simulated self-bias voltages given in the caption also correspond well. The self-bias values are negative as expected for an excitation electrode smaller than the ground electrode [28].

Figs. 4(a) and (b) show the corresponding measurement and numerical solution (using Eq. (18)) for the dc current density $J(\underline{x})$ flowing to the ground electrode for the same plasma conditions as in Fig. 3. This current is due to local non-ambipolarity caused by an rf amplitude spatial variation in the presence of a constant dc plasma potential and the constant potential of a conducting electrode, as shown in Fig. 6 of Ref. [1] for the equivalent one-dimensional case. There is a net positive ion current to the ground electrode periphery and sidewalls, compensated by a net electron current to the central region. The dc current per unit area, J, entering the electrode normally from the plasma, is the source term for a dc current per unit width, $\vec{j}_w$, which flows laterally across the ground electrode. Continuity of this dc current circulating through the plasma via the conducting electrode requires that $\nabla \cdot \vec{j}_w = J$. Circulating dc current was also observed in a high frequency capacitive reactor where the rf amplitude spatial variation was due to the standing wave effect [18, 25]. Global ambipolarity, imposed by capacitive coupling in the external rf circuit, means that the surface integral of the dc current J to the ground electrode (including the sidewall current) must be zero. This is assured in the numerical solution, Fig. 4(b), by adjustment of the dc plasma potential. Experimentally, the surface integral interpolated from the measured dc probe current in Fig. 4(a) is only approximately zero ($\Sigma \bar{I}_{gnd}/\Sigma|\bar{I}_{gnd}| = -15\%$) which indicates the degree of approximation of the probe method used.

The probe saturated current spatial profile in Fig. 4 (c) would ideally be flat since the experiment is compared with a model which assumes uniform plasma density and electron temperature. In practice, the per cent relative standard deviation over the surface interpolated from the measurements in Fig. 4 (c) is 14%. The discrepancy between the measurement and the uniform model is probably due to the approximation inherent in the probe technique and to the nonuniformity of the plasma itself.

The probe measurements in Fig. 4(a) of the dc current circulating between the plasma and the ground electrode agree reasonably well with the predictions of the telegraph model in Fig. 4(b). In general, however, the probe current measurements gave less satisfactory comparisons with the numerical solutions than the voltage measurements. This might be because the current measurements are small ($\sim 60\mu$A for each probe in Fig. 4 (c)) making them susceptible to stray leakage currents and to any surface contamination of the probes. Furthermore, comparison of the current measurements with the numerical solution for the voltage involves a strongly non-linear relation (Eq. (18)). Therefore, from now on, only the voltage measurements will be shown since these represent the most direct comparison with the numerical solution of the telegraph equation for the voltage.

Figs. 5(a) and (b) show the measurement and numerical solution of the plasma potential rf amplitude spatial dependence for the same reactor geometry as in Fig. 3, but for a long damping length, δ =105 mm. Now, the influence of the area-asymmetry at the corners extends over almost the whole reactor surface, as seen on both graphs, because the telegraph perturbation distance $\approx 3\delta = 315$ mm is longer than the reactor half-widths. The relative magnitude of the plasma potential variation, $\Delta\tilde{u}_p/(\tilde{u}_{rf}/2)$ is again $\approx 20\%$. The one-dimensional model [1] also predicts a longer range, but a smaller amplitude for the perturbation; the discrepancy is due to the two-dimensional effect via the influence of the corners which is correctly accounted for in the two-dimensional numerical solution. The lower pressure used means that $\omega/\nu = 0.284$ is no longer much less than one and so the inductive term in Eqs. (21) and (22) begins to introduce a spatial oscillation into the borders of the simulated plasma potential rf amplitude variation in Fig. 5(b). The spatial resolution of the probe array is insufficient to observe this, but the measurement and numerical solution are again in general agreement for the form and amplitude of the rf amplitude spatial dependence. The shift in the dc plasma potential differs by about 4.5 V between measurement and numerical solution, and this is also observed in the 4.5 V discrepancy between the self-bias values.

B. Inverse asymmetry: ground electrode area smaller than the excitation electrode area

The asymmetry shown schematically in Fig. 6 is inverted with respect to Fig. 3 by adding sidewalls to all four sides of the excitation electrode. The plasma is now laterally confined by sidewalls at the excitation electrode potential instead of ground, and so the effective grounded area is now smaller than the excitation electrode area.

For comparison with Figs. 3(a) and (b), Figs. 6(a) and (b) represent the inverse asymmetry measurement and numerical solution of the spatial dependence of the plasma potential rf amplitude, for short damping length, δ =33 mm. The inverted asymmetry means that the sign of the sidewall current perturbation in the telegraph model, Eq. (24), is reversed. The observed inversion of the voltage profile therefore supports the validity of

the telegraph description. Note that both the measurement and numerical solution for inverse asymmetry are not exact mirror images of Fig. 3 because, although the sum of the ground and excitation sheath voltages always equals the applied excitation voltage, the varying phase of the propagating telegraph mode means that this does not hold for the sum of their amplitudes. Explicitly, the perturbation magnitude for the symmetry in Sec. IV A, $\triangle\tilde{u}_p = |\tilde{u}_{rf}/2 + \tilde{\mathrm{v}}(\underline{x})| - \tilde{u}_{rf}/2$, is not the exact mirror image of the perturbation magnitude for the inverse symmetry of this section, $\triangle\tilde{u}_p = |\tilde{u}_{rf}/2 - \tilde{\mathrm{v}}(\underline{x})| - \tilde{u}_{rf}/2$, because of the phase variation of $\tilde{\mathrm{v}}(\underline{x})$ with respect to the rf excitation.

The measured and modeled self-bias values are of similar magnitude to the previous reactor symmetry of Fig. 3, but are now *positive* as expected when the excitation electrode is *larger* than the ground electrode [28].

Fig. 7 is the inverse asymmetry version of Fig. 5 for long damping length, δ =105 mm, which also confirms the inversion of the plasma potential perturbation and of the self-bias voltage, according to the telegraph effect. Incidentally, this inversion shows that the dome profile in Fig. 5 is not associated with the standing-wave effect, because otherwise the rf excitation voltage and both sheath voltage perturbations would all have a central maximum independently of the reactor symmetry [11, 13]. Conversely, in the telegraph effect, the sheath voltage perturbations are equal and opposite, with the central maximum of the sheath voltage occurring at the larger-area electrode, and a minimum at the smaller-area electrode, as observed. The only major discrepancy between measurement and telegraph numerical solution is again a difference of a few volts in the dc levels of the plasma potential and self-bias.

C. Symmetric reactor

This is the trivial case for which the telegraph effect should vanish, leaving no perturbation to the rf plasma potential, because the sum of the injected ground and excitation rf currents from the equal-height sidewalls is zero [1], i.e. the net sidewall current $I|_{wall} = 0$ in Eq. (24). All the probe dc voltages, $\bar{V}_f$, and dc currents, $\bar{I}_{gnd}$, should then be zero, including the self-bias, and Eq. (5) satisfied everywhere. The measured perturbations in Fig. 8(a) (short damping length) and (b) (long damping length) are, on the whole, considerably smaller than the asymmetric cases in Figs. 3(a), 6(a) and Figs. 5(a), 7(a) respectively, but not zero. This is possibly due in part to imperfect electrode symmetry: the 12.5 mm sidewall heights are equal on all four sides, but the ground electrode remains slightly wider than the excitation electrode. The most obvious nonuniformities are close to the corners in Fig. 8(a): the added sidewalls were not perfectly aligned, leaving small gaps where spurious, 'parasitic' plasma could exist.

The measured self-bias for the long-δ plasma, Fig. 8(b), was 0 V as expected for a symmetric reactor. However, the magnitude of the +2 V self-bias for the short-δ plasma in Fig. 8(a) was no smaller than for the asymmetric cases, Figs. 3(a) and 6(a). Since the self-bias voltage depends on the plasma currents integrated over the whole surface of both electrodes, it is influenced by any spurious plasma nonuniformity, such as apparently exists in the corners of Fig. 8(a). Nevertheless, it seems clear that accurate symmetrization of the ground and excitation electrodes would help to give a uniform rf plasma potential, as predicted by the telegraph theory. A symmetric electrode design is therefore advantageous for plasma processing from the point of view of uniform plasma potential and sheath voltages.

D. Quantitative comparison with the telegraph analytical model

To quantitatively test the telegraph one-dimensional analytical model in Ref. [1], we consider the line profile of plasma potential rf amplitude across an axis of the reactor (y =0 to 470 mm at x =285 mm) for short damping length, $\delta \approx 33$ mm, using the asymmetric reactor results in Secs. IV A and IV B. Case A in Fig. 9 superposes the voltage measurements for the probes closest to this axis from Fig. 3(a) with the corresponding line profiles from the two-dimensional solution in Fig. 3(b) and the one-dimensional analytical solution from Ref. [1] (see below). Case B in Fig. 9 superposes the corresponding line profiles for the inverse reactor asymmetry from Fig. 6. All the profiles are set to zero at the electrode center.

These profiles for the short damping length case are appropriate for comparison with the one-dimensional solution because the electrode half-width of the perpendicular axis, 285 mm, is sufficiently longer than the telegraph perturbation distance $\sim 3\delta$ =99 mm, so that the proximity of the lateral walls does not invalidate the assumption of a one-dimensional plasma model [1] along the short axis. Furthermore, $\omega/\nu_m = 0.085 \ll 1$ so that the resistive approximation made for the model in Ref. [1] is also valid for these plasma conditions. The comparison for the symmetrical reactor of Sec. IV C is not added to Fig. 9 because the trivial result for zero perturbation gives no quantitative test of the analytical model.

The one-dimensional resistive model line profile for the plasma potential rf amplitude is given by the magnitude of

$$\tilde{\mathbf{u}}_p(x) = \frac{\tilde{u}_{rf}}{2}\left[1 - K\cosh(\gamma x)\right]; K = \frac{H}{(2/\gamma)\sinh(\gamma L) + H\cosh(\gamma L)} \quad (27)$$

from Ref. [1] Eq. (14), where $\gamma = (1+i)/\delta$. The relevant parameters for the analytical profiles in Fig. 9, Cases A and B, are the damping length $\delta = 33$ mm, the reactor half-width $L = 235$ mm, and the rf excitation amplitude $\tilde{u}_{rf} = 24$ V. The effective sidewall height in contact with the plasma is $|H| = (25 - 2d)/1.5$ mm where $d = 4$ mm is the sheath width and the factor 1.5 accounts for the

wall effective sheath width, $d_{wall} = 1.5d$. These parameters are identical to those used for the two-dimensional numerical simulation. For Case A (grounded sidewall), $H = +|H|$; and for Case B (sidewall connected to the excitation electrode), $H = -|H|$.

The measurements, the two-dimensional numerical solution and the one-dimensional analytical solution are in very good agreement in Fig. 9, thus giving a quantitative confirmation of the telegraph model in Ref. [1].

The long damping length case, $\delta \approx 105$ mm, is influenced by the lateral walls [18] because the telegraph perturbation distance $\sim 3\delta \approx 315$ mm is longer than the reactor half-widths. The one-dimensional model would consequently underestimate the size of the measured perturbations, whereas the two-dimensional numerical solution satisfactorily reproduces the experimental results in Figs. 5 and 7.

Up till now, it has not been considered whether the edge-localized (fringing field) modes [9], which co-exist with the telegraph mode [1], are also influencing the measurements of the plasma potential perturbation. The distinction between the telegraph mode and edge-localized modes can be deduced as follows: (i) The observed suppression of the plasma potential perturbation due to symmetrization of the electrodes is explained by the telegraph effect, whereas a fringing field perturbation would not be strongly reduced by the sidewall symmetrization [1]; and ii) The plasma potential perturbation is observed to penetrate far into the reactor interior - depending on plasma conditions - which can be explained by the telegraph mode propagating inwards from asymmetric sidewalls. On the other hand, the fringing field perturbation does not propagate and remains localized within $h/\pi < 8$ mm of the electrode junction at the sidewall [9]. The probes are not close enough to the reactor edge to be strongly influenced by the edge-localized modes.

In conclusion, it is reasonable to assume that the measured perturbations to the plasma potential rf amplitude are principally due to the telegraph effect.

E. Surface potential on a dielectric substrate in an asymmetric reactor

A surprising prediction of the telegraph effect is the *negative* surface potential of a thin dielectric substrate, placed on the ground electrode, when exposed to plasma in an asymmetric reactor where the ground electrode has the larger area [1]. If the plasma dc and rf potentials were uniform, capacitive division of the plasma potential (which is always positive with respect to all surfaces) between the sheath capacitance and the dielectric substrate capacitance would only ever allow for a *positive* surface potential.

The surface potential was measured for a 1 mm-thick glass substrate, 470 mm $\times$ 370 mm, positioned centrally on the ground electrode for the conventional reactor asymmetry of Sec. IV A. Circular holes were cut in the glass, aligned with the array of large probes, to expose the metal probe heads. Since the glass surface is electrically floating, the probe dc floating potential gives an estimate for the substrate surface potential (this is only approximate because the rf potential of the glass surface is not exactly zero - the case of non-zero dielectric thickness is considered in Sec. III E of Ref. [1]). Fig. 10(a) shows this approximate substrate surface potential measured directly from the probe floating potentials: it is negative, as predicted by the telegraph effect, over all the substrate except for its corners. The 50 mm-wide exposed border of the conducting ground electrode is at 0 V.

For comparison, the substrate surface potential can be calculated from the difference between the uniform dc plasma potential and the dc self-rectification voltage of the sheath at the substrate [25]. The dc plasma potential must be downshifted in presence of the substrate to guarantee global ambipolarity over the conducting border of the ground electrode where the rf sheath voltage is lower due to the telegraph effect. The rf sheath voltage is larger towards the center of the reactor, following the telegraph profile, and so the sheath dc self-rectification voltage above the insulating substrate is now larger than the dc plasma potential. Their difference therefore predicts a negative substrate surface potential. The calculated substrate surface potential in Fig. 10(b) agrees reasonably well with the measurements in Fig. 10(a), which qualitatively confirms the telegraph model. The measured and calculated substrate potential, using $\delta \simeq 70$ mm, is bipolar due to the two-dimensional influence of the reactor corners extending onto the substrate corners. The downshift in dc plasma potential also drives the self-bias downwards to maintain global ambipolarity over the excitation electrode (see Sec. III C in Ref. [1]), which explains the measured self-bias decrease from -8 V without substrate, to -18 V with the substrate.

A spatial variation in dc sheath voltage across the surface of a dielectric substrate in an asymmetric reactor would result in nonuniform ion energy bombardment, which could be a critical issue for etch uniformity [25]. According to the simulation performed for Fig. 10(b), the ion bombardment energy would vary from 67 eV at the reactor edge to 78 eV at the substrate center, with a discontinuity in ion energy at the electrode-substrate boundary of up to 7 eV at the reactor axes. Such a sheath voltage discontinuity has been experimentally shown to be accompanied by a lateral electric field over the substrate surface for a few mm at its edge [29].

A negative substrate surface potential is also confirmed by measurements of a negative substrate charge using the same reactor configuration [30]. This negative charge, inexplicable in terms of a unique plasma potential, corroborates the telegraph effect. Finally, the glass surface potential was measured to be positive for the inverse asymmetry of Sec. IV B, as expected from the telegraph model.

V. CONCLUSIONS

A surface array of unbiased electrostatic probes was used for experimental verification of the spatial dependence of the plasma potential rf amplitude predicted by the telegraph effect in a large area, asymmetric capacitive plasma reactor. The telegraph effect is caused by the redistribution of rf current near asymmetric sidewalls to maintain rf current continuity between the electrodes - this causes a rf plasma potential perturbation to propagate laterally across the plasma. The resulting perturbation to the edge plasma can be significant even for sidewall heights which are much smaller than the electrode width. The telegraph electromagnetic mode is different from the standing wave and edge-localized modes [13] and occurs even at low excitation frequencies.

The negative of the probes' dc floating potential in the surface of the ground electrode was shown to give an approximate measurement of the plasma potential rf amplitude perturbation which was compared with a two-dimensional solution of the telegraph equation. The predictions of the telegraph theory [1, 2] are confirmed by the probe experiments as follows: i) The spatial dependence of the plasma potential perturbation given by the numerical solution of the telegraph equation is observed by experiment for both short and long damping lengths. The spatial profile is inverted when the electrode area asymmetry is inverted, and the variation is strongly reduced when the areas are closely symmetric; ii) A circulating dc current between the plasma and the ground electrode is observed; iii) The surface potential of a thin dielectric substrate placed on a grounded, larger-area electrode is confirmed to be negative.

The practical significance of the telegraph effect was recently demonstrated by the nonuniformity of film thickness during plasma-enhanced chemical vapor deposition in an asymmetric large area reactor, as shown in two papers [31, 32] submitted during the writing of this article. In conclusion, a symmetric electrode design is advantageous for large-area plasma processing uniformity from the point of view of uniform plasma potential and sheath voltages.

Acknowledgments

This work was funded by Swiss Federal Research Grant CTI 5994.2 and performed with the collaboration of Unaxis Displays in Palaiseau, France, and Truebbach, Switzerland.

APPENDIX: ACCURACY OF THE UNBIASED PROBE METHOD

The spatial variation of the probe floating dc negative potential, $-\triangle\bar{V}_f(\underline{x})$, is approximated to the spatial variation of the plasma potential rf amplitude perturbation, $\triangle\tilde{u}_p(\underline{x})$, in Eq. (14) and in the experimental results. Here, we estimate the accuracy of the successive approximations used in deriving Eq. (14). Consider Eq. (5), which is exact for a sinusoidal sheath voltage, with the substitutions $X = \bar{U}_{sym}/T_e$ and $x = \tilde{u}_p/T_e = \tilde{u}_{rf}/2T_e$. The rate of change of the sheath dc potential with respect to the sheath rf amplitude, $\partial X/\partial x = -\partial\bar{V}_f/\partial\tilde{u}_p$, is

$$\partial X/\partial x = \mathbf{I}_0'(x)/\mathbf{I}_0(x) = \mathbf{I}_1(x)/\mathbf{I}_0(x), \qquad \text{(A.1)}$$

where $\mathbf{I}_1(x)$ and $\mathbf{I}_0(x)$ are respectively the first and zeroth orders of the modified Bessel function of the first kind [23]. From the asymptotic expansion in Eq. 6 we obtain

$$\partial X/\partial x \simeq 1 - 1/2x \text{ for } x > 5. \qquad \text{(A.2)}$$

The approximation used for the experimental results, Eq. (14), gives

$$\partial X/\partial x \approx 1 \text{ for } x > 5. \qquad \text{(A.3)}$$

Eqs. (A.1) - (A.3) are expressions for the 'constant of proportionality' between $-\triangle\bar{V}_f$ and $\triangle\tilde{u}_p$. As shown in Fig. 11, the approximation $-\triangle\bar{V}_f \approx \triangle\tilde{u}_p$ is an overestimate for the first two expressions, but not by more than 10 %.

The sheath voltage has been assumed to be purely sinusoidal up till now. To estimate the influence of sheath voltage harmonics, we use an analytical solution for the capacitive rf sheath by Lieberman [33] which includes the second and third voltage harmonics. For this case, the $\cos\omega t$ time dependence in Eq. (1) is replaced by $\cos\omega t + 0.123\cos 2\omega t - 0.042\cos 3\omega t$. Expressions A.1-A.3 are plotted for comparison in Fig. 11 along with a numerical evaluation for $\partial X/\partial x$ accounting for these sheath voltage harmonics. In conclusion, the spatial variation of the probe floating dc negative potential, $-\triangle\bar{V}_f(\underline{x})$, approximately represents the spatial variation of the plasma potential rf amplitude perturbation, $\triangle\tilde{u}_p(\underline{x})$, even in the presence of weak harmonics of the sheath rf voltage, to an estimated accuracy of $\pm 10\%$. This is sufficiently accurate for this experimental investigation of the telegraph effect, especially since this is a systematic error which does not change the form of the measured voltage distributions.

REFERENCES

[1] A. A. Howling, L. Sansonnens, J. Ballutaud, C. Hollenstein, and J. P. M. Schmitt, J. Appl. Phys. **96**, 5429 (2004).

[2] J. P. M. Schmitt, M. Elyaakoubi, and L. Sansonnens, Pl. Sources Sci. Technol. **11**, A206 (2002).

[3] L. Sansonnens, J. Bondkowski, S. Mousel, J. P. M. Schmitt, and V. Cassagne, Thin Solid Films **427**, 21 (2003).

[4] G. S. Selwyn, J. E. Heidenreich, K. L. Haller, and J. J. Wu, J. Vac. Sci. Technol. A **9**, 37 (1991).

[5] C. Hollenstein, A. A. Howling, C. Courteille, J.-L. Dorier, L. Sansonnens, D. Magni, and H. Müller, Mat. Res. Soc. Symp. Proc. **507**, 547 (1998).

[6] J. P. M. Schmitt, Thin Solid Films **174**, 193 (1989).

[7] J. P. M. Schmitt, Mat. Res. Soc. Symp. Proc **219**, 631 (1991).

[8] L. Sansonnens, A. Pletzer, D. Magni, A. A. Howling, C. Hollenstein, and J. P. M. Schmitt, Plasma Sources Sci. Technol. **6**, 170 (1997).

[9] M. A. Lieberman, J. P. Booth, P. Chabert, J. M. Rax, and M. M. Turner, Plasma Sources Sci. Technol. **11**, 283 (2002).

[10] L. Sansonnens and J. Schmitt, Appl. Phys. Lett. **82**, 182 (2003).

[11] A. Perret, P. Chabert, J.-P. Booth, J. Jolly, J. Guillon, and P. Auvray, Appl. Phys. Lett. **83**, 243 (2003).

[12] P. Chabert, J.-L. Raimbault, J. M. Rax, and M. A. Lieberman, Phys. Plasmas **11**, 1775 (2004).

[13] H. Schmidt, L. Sansonnens, A. A. Howling, C. Hollenstein, M. Elyaakoubi, and J. P. M. Schmitt, J. Appl. Phys. **95**, 4559 (2004).

[14] P. Chabert, J.-L. Raimbault, J. M. Rax, and A. Perret, Phys. Plasmas **11**, 4081 (2004).

[15] V. A. Godyak and R. Piejak, J. Appl. Phys. **68**, 3157 (1990).

[16] A. Dyson, P. Bryant, and J. E. Allen, Meas. Sci. Technol. **11**, 554 (2000).

[17] K. Teii, M. Mizumura, S. Matsumura, and S. Teii, J. Appl. Phys. **93**, 5888 (2003).

[18] J. Ballutaud, C. Hollenstein, A. A. Howling, L. Sansonnens, H. Schmidt, and J. P. M. Schmitt, Proceedings of the 16th Int. Symp. Pl. Chem. ISPC16, June 22-27 (2003), Taormina, Italy, CD-ROM published by the Organizing Committee, edited by R. D'Agostino (Universita degli Studi di Bari, Bari, Italy) (2003).

[19] A. Garscadden and K. G. Emeleus, Proc. Phys. Soc. **79**, 535 (1962).

[20] H. S. Butler and G. S. Kino, Phys. Fluids **6**, 1346 (1963).

[21] K.-U. Riemann, J. Appl. Phys. **65**, 999 (1989).

[22] M. A. Lieberman and A. J. Lichtenberg, *Principles of Plasma Discharges and Materials Processing* (John Wiley and Sons, New York, 1994).

[23] M. Abramowitz and I. A. Stegun, *Handbook of Mathematical Functions* (Dover, New York, 1965).

[24] A. Perret, P. Chabert, J. Jolly, and J.-P. Booth, Appl. Phys. Lett. **86**, 021501 (2005).

[25] A. A. Howling, L. Sansonnens, H. Schmidt, and C. Hollenstein, Comment submitted to Appl. Phys. Lett. Jan. (2005).

[26] G. Mümken and U. Kortshagen, J. Appl. Phys. **80**, 6639 (1996).

[27] D. T. Sandwell, Geophys. Res. Lett. **14**, 139 (1987).

[28] K. Köhler, J. W. Cobrun, D. E. Horne, E. Kay, and J. H. Keller, J. Appl. Phys. **57**, 59 (1985).

[29] E. V. Barnat and G. A. Hebner, Appl. Phys. Lett. **85**, 3393 (2004).

[30] A. A. Howling, A. Belinger, P. Bulkin, L. Delaunay, M. Elyaakoubi, C. Hollenstein, J. Perrin, L. Sansonnens, J. Schmitt, and E. Turlot, Proc. 15th Int. Symp. Plasma Chemistry, Orleans, France **1**, 33 (2001).

[31] L. Sansonnens, B. Strahm, L. Derendinger, A. A. Howling, C. Hollenstein, C. Ellert, and J. P. M. Schmitt, to appear in J. Vac. Sci. Technol. **A** (2005).

[32] R. Sobbia, L. Sansonnens, and J. Bondkowski, to appear in J. Vac. Sci. Technol. **A** (2005).

[33] M. A. Lieberman, IEEE Trans. Plasma Sci **16**, 638 (1988).

FIGURE CAPTIONS

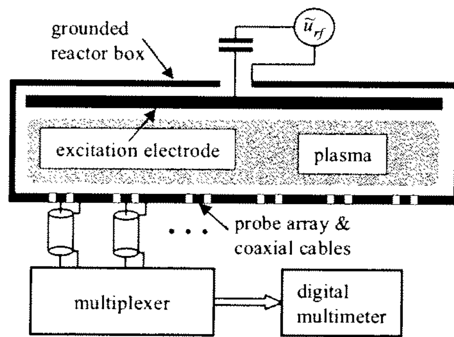

FIG. 1: Schematic of the reactor, probe array and acquisition block diagram for dc voltage and dc current measurements. The
mea

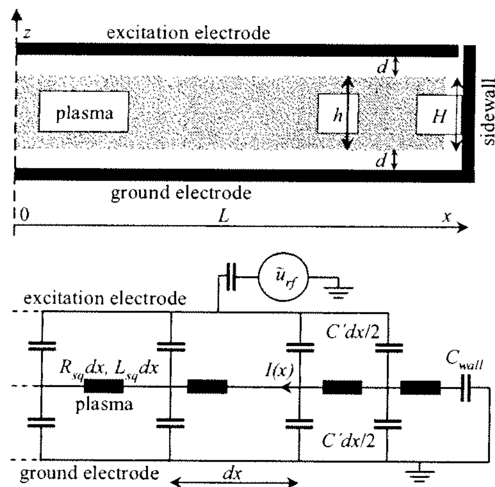

FIG. 2: Above: Schematic of the plasma and electrode geometry, showing a half-width L with a grounded sidewall. Below: Equivalent circuit of the plasma and sheath impedances [1].

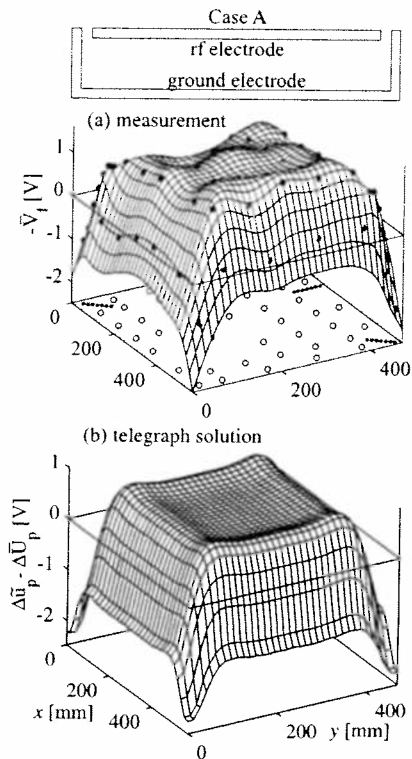

FIG. 3: Top: Schematic of the asymmetric reactor geometry (not to scale). The graphs show the perturbation to the plasma potential rf amplitude with respect to a symmetric reactor, for short telegraph damping length $\delta = 33$ mm: (a) probe negative dc floating potential measurements (the black points indicate the data points on the interpolated surface and the white points show the $\{x, y\}$ positions of the probes); (b) numerical solution of the telegraph equation. Rf amplitude $\tilde{u}_{rf} = 24.4$ V. The measured and simulated self-bias voltages are -1.5 V and -1.2 V respectively. Plasma parameters are given in Sec. IV.

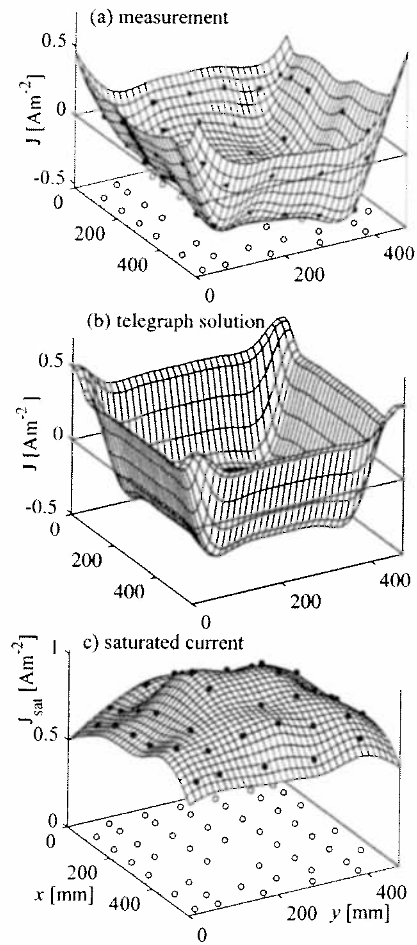

FIG. 4: Dc current density to the ground electrode surface for the same reactor asymmetry and plasma conditions as in Fig. 3 with the same short telegraph damping length $\delta = 33$ mm: (a) measurements of dc current with unbiased probes; (b) numerical solution of the telegraph equation; (c) measurement of the ion saturated current density spatial profile.

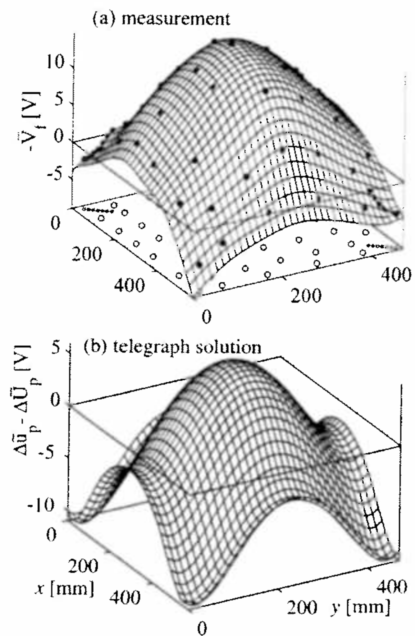

FIG. 5: For the same reactor asymmetry as in Fig. 3, the graphs show the perturbation to the plasma potential rf amplitude with respect to a symmetric reactor, for plasma conditions with a long telegraph damping length δ = 105 mm: (a) probe negative dc floating potential measurements; (b) numerical solution of the telegraph equation. Rf amplitude $\tilde{u}_{rf}$ = 140 V. The measured and simulated self-bias voltages are -17.5 V and -13 V respectively. Plasma parameters are given in Sec. IV.

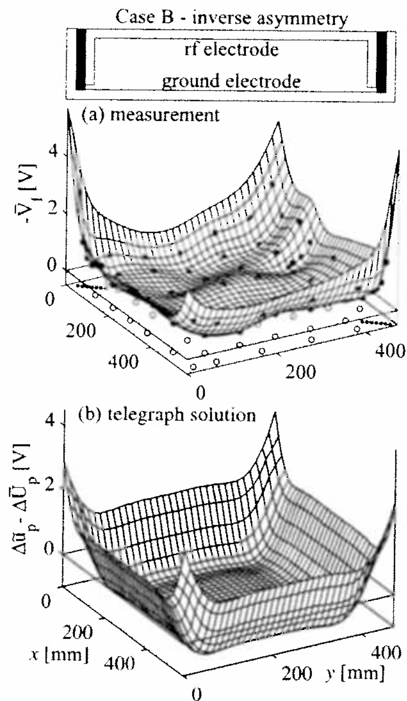

FIG. 6: Top: Schematic of the reactor with inverse asymmetry compared to Fig. 3 (not to scale). The black rectangles represent dielectric inserts to prevent parasitic plasma behind the added sidewalls. The graphs show the perturbation to the plasma potential rf amplitude with respect to a symmetric reactor, for short telegraph damping length $\delta = 33$ mm: (a) probe negative dc floating potential measurements; (b) numerical solution of the telegraph equation. Rf amplitude $\tilde{u}_{rf} = 23.2$ V. The measured and simulated self-bias voltages are +2 V and +1.5 V respectively. Plasma parameters are given in Sec. IV.

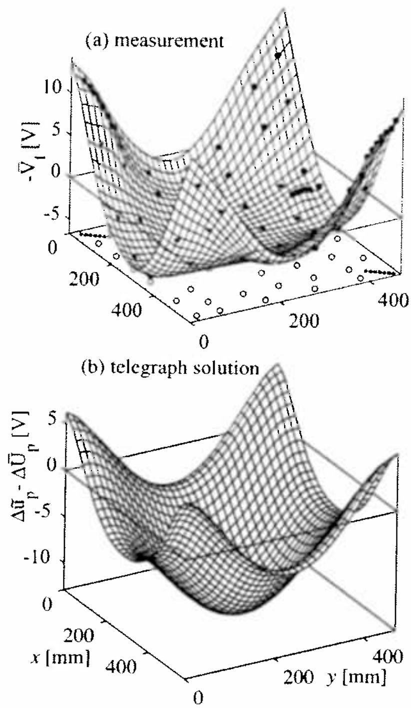

FIG. 7: For the same reactor inverse asymmetry as in Fig. 6, but for plasma conditions with long damping length $\delta = 105$ mm: (a) probe negative dc floating potential measurements; (b) numerical solution of the telegraph equation. Rf amplitude $\tilde{u}_{rf} = 141$ V. The measured and simulated self-bias voltages are +23 V and +15 V respectively. Plasma parameters are given in Sec. IV.

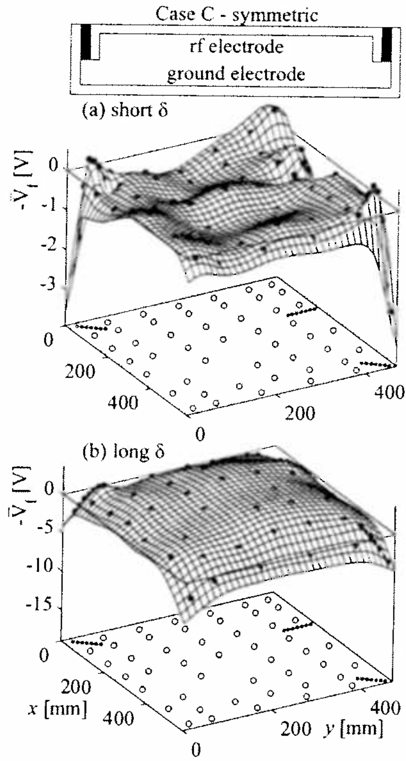

FIG. 8: Top: Schematic of the reactor with symmetric electrode areas (not to scale). The black rectangles represent dielectric inserts to prevent parasitic plasma behind the added, half-height sidewalls. (a) probe negative dc floating potential measurements for short damping length δ =33 mm (rf amplitude $\tilde{u}_{rf}$ = 22.2 V, self-bias voltage +2 V); (b) probe negative dc floating potential measurements for long damping length δ =105 mm (rf amplitude $\tilde{u}_{rf}$ = 92 V, self-bias voltage 0 V).

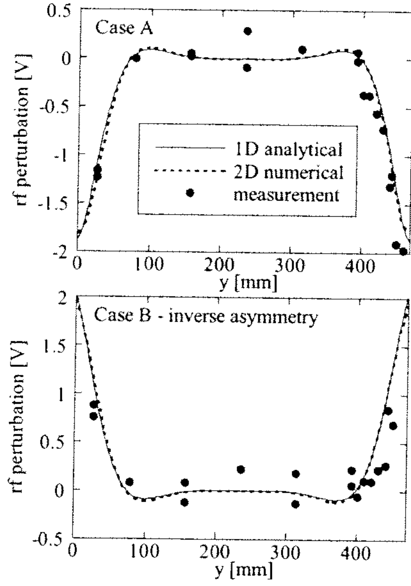

FIG. 9: Line profiles of the spatial perturbation to the plasma potential rf amplitude across the reactor short axis for short damping length δ =33 mm. Case A: for the reactor asymmetry in Sec. IV A; Case B: for the inverse asymmetry in Sec. IV B. Each graph compares the measurements with the two-dimensional numerical solution and the one-dimensional analytical solution [1] of the telegraph equation.

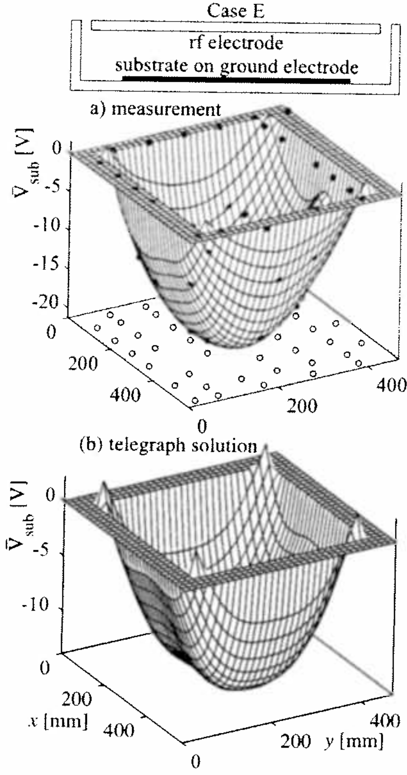

FIG. 10: Top: Schematic of the asymmetric reactor with a dielectric substrate (not to scale). (a) the measured surface potential across the ground electrode including the dielectric substrate; (b) the calculated surface potential, using the two-dimensional numerical solution of the telegraph equation (with δ =70 mm) and the self-rectification condition for the sheath at the substrate. Rf amplitude $\tilde{u}_{rf}$ = 140 V.

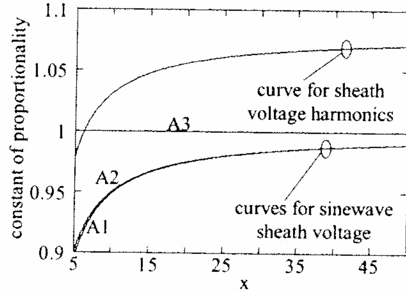

FIG. 11: Comparison of the expressions for $\partial X/\partial x = -\partial \bar{V}_f/\partial \tilde{u}_p$ in Eqs. A.1-A.3, and for sheath voltage harmonics. The estimated error in assuming that $-\Delta \bar{V}_f \approx \Delta \tilde{u}_p$ for the probe measurements is less than $\pm 10\%$. Low rf power experiments for $\delta = 33$ mm correspond to $5 < x = \tilde{u}_p/T_e < 7$ (for $T_e = 2$ V); high rf power experiments for $\delta = 105$ mm correspond to $27 < x < 43$.